J. Fluid Mech. (2004), *vol.* 507, *pp.* 43–69.
DOI: 10.1017/S0022112004008110 Printed in the United Kingdom

Similarity laws of velocity profiles and turbulence characteristics of Couette–Poiseuille turbulent flows

By KOICHI NAKABAYASHI[1]†, OSAMI KITOH[1] AND YOSHITAKA KATOH[2]

[1]Department of Mechanical Engineering, Nagoya Institute of Technology, Gokiso-cho, Showa-ku, Nagoya 466-8555, Japan

[2]Toyota Communication System Co., Ltd. Higashi-Sakura Daiichi Bldg. 7F, Higashi-Sakura, Higashi-ku, Nagoya 461-0005, Japan

(Received 5 February 2003 and in revised form 13 November 2003)

Similarity laws of mean velocity profiles and turbulence characteristics of Couette–Poiseuille turbulent flow (C-P flow) have been studied experimentally. The global parameters of C-P flow are the Reynolds number Re^* and the dimensionless shear stress gradient μ and flow parameter β. The effects of these parameters on the turbulence structure have also been considered in the wall region and turbulent core region, respectively. In the wall region, the wall law varies greatly with μ but slightly with Re^*. Typically, the additive constant B of the logarithmic law (or Van Driest damping factor A^+) is shown to depend only on μ. Turbulence characteristics are also strongly influenced by μ, but not much by Re^*. Because the relation $\mu = -Re^*$ holds in plane Poiseuille flow and Re^* has little effect on the similarity laws for C-P flows, the low-Reynolds-number effect on the additive constant and turbulence quantities for plane Poiseuille flow can be attributed to the μ effect. In the turbulent core region, however, there is a great difference in the defect law of the velocity profile and the distribution of turbulence intensity between Poiseuille (P)- and Couette (C)-types flows. For P-type flow, an effective friction velocity u_e^* and a new coordinate $\eta = y - h_s$ are recommended for the universal profile, where $y = h_s = \delta_p$ is the position of $\tau = 0$ and δ_p is considered to be appropriate as a characteristic length scale of turbulence. For C-type flow, a different effective friction velocity $u_{c,}^*$ the characteristic length scale $2h$ and the wall coordinate y are preferred. The turbulence activity away from the wall is extremely high for $\mu > 0$ and low for $\mu < 0$. A strong sweep event plays a dominant role in the Reynolds shear stress when $0 < \mu < 50$, whereas strong ejection from the near-wall region prevails in the case of negative μ with a small absolute value.

1. Introduction

Turbulent Couette–Poiseuille (C-P) flow has a number of applications in engineering practice. The most obvious is in predicting the motion within turbulent bearing films. The usual approximation of lubrication theory represents bearing films by splicing

† Present address: Department of Mechanical System Engineering, Aichi University of Technology, 50-2 Manori, Nisihazama-cho, Gamagori-city, Aichi Pref., 443-0047, Japan.

together a series of fully developed C-P flows. Two particular C-P flows, i.e. pure pressure or plane Poiseuille flow and pure shearing or plane Couette flow, have been studied so far. However, except for El Telbany & Reynolds (1980, 1981), combined C-P flow has not been investigated.

Many studies have been conducted on the similarity laws for turbulent boundary layers with a pressure gradient, for example Kays (1971), Kader & Yaglom (1978), Blackwelder & Kovasznay (1972) and Nagano, Tagawa & Tsuji (1991). In particular, Kader & Yaglom (1978) carefully examined and compared the results for many developing boundary layers exposed to adverse pressure gradients in order to note points of disagreement, and deduced similarity laws that described many such flows with good accuracy. They adopted the streamwise gradient of kinematic pressure, $\mathrm{d}p/\mathrm{d}x/\rho$, as the parameter characterizing the departure of a boundary layer from the constant stress pattern in the constant stress layer. Since the local shear stress plays an important role in the turbulence intensities and dynamic aspects of the turbulence, El Telbany & Reynolds (1980) adopted the wall-normal shear stress gradient $\partial\tau/\partial y$ as the relevant dynamic parameter. They concluded that $\partial\tau/\partial y$ should be adopted in developing a unified view of the wall layer, applicable to both channel and boundary layer flows. In the boundary layer flow, however, $\partial\tau/\partial y$ is not constant, but varies in the wall-normal direction. On the other hand, for fully developed channel flow, $\partial\tau/\partial y$ is constant in the whole flow region. Consequently, C-P flow is the best flow in which to investigate the effect of the shear stress gradient on the similarity law of the velocity profile and the turbulence intensity. This is the main reason why we investigate C-P flow here.

In a study of the similarity laws of velocity profiles and turbulence characteristics in C-P flow, the work by El Telbany & Reynolds may be considered a typical experimental investigation, although Thurlow & Klewicki (2000) reported an investigation on the so-called 'geometry effect' recently. Kuroda, Kasagi & Hirata (1994), on the other hand, studied the effect of mean shear rate on the wall turbulence by numerical simulation. But no systematic studies on the velocity profiles and turbulence statistics on C-P flows have been published so far except for that by El Telbany & Reynolds. However the inlet length influenced their measurements, so the present investigation has been conducted for the fully developed condition.

The main objective of this work is to clarify the effect of shear stress gradient on the velocity profiles and characteristics of wall turbulence. The global parameters of C-P flows are the Reynolds number $Re^* = u_s^* h/\nu$, the dimensionless shear stress gradient $\mu = u_s^{*3}/(\alpha\nu)$ and the flow type $\beta = \alpha h/u_s^{*2}$. Here ν is the viscosity and, u_s^*, h, $\alpha = \mathrm{d}(\tau/\rho)/\mathrm{d}y$ and y stand for the friction velocity based on the shear stress at the stationary wall, the channel half-height, the kinematic shear stress gradient and the distance from the stationary wall. The values of these parameters can be changed independently by selecting various combinations of bulk flow velocity (flow rate) and moving-wall speed in the C-P flow. Thus we can investigate the effect of each of these parameters on the similarity laws of turbulence statistics separately. However, plane Poiseuille flow, a particular case of C-P flow, has a relation of $Re^* = -\mu$. Accordingly, we cannot set different values of Re^* and μ in plane Poiseuille flow.

In the present paper, we first give an overview of C-P flows in § 2. Since the flows under consideration are classified into Poiseuille and Couette types, we shall discuss the difference between the two types. Also, we discuss dividing the flow into regions for consideration of the velocity defect law in the turbulent core region. In § 3, the experimental apparatus and method are described. Wall friction is considered in § 4. In § 5, similarity laws of mean velocity profiles are discussed within the basic scheme

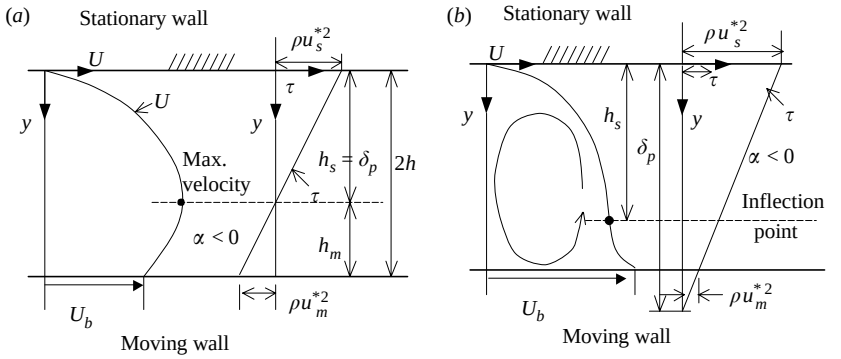

FIGURE 1. Schematics of mean velocity profiles and shear stress distributions: (*a*) P-type flow, (*b*) C-type flow.

considered in § 2. Similarity laws of turbulence intensities, correlation coefficient, skewness factor and four-quadrant analysis of Reynolds shear stress are discussed in § 6.

2. Poiseuille and Couette flow types

The C-P flow can be divided into the Poiseuille-type (P-type) and Couette-type (C-type), as shown in figure 1, by whether there is a region of zero shear stress in the flow between two walls. The upper wall is stationary and the lower wall is moving. The subscripts s and m denote the stationary and moving walls, respectively. In P-type flow, a position at which $\tau = 0$, i.e. $y = \delta_p = u_s^{*2}/|\alpha|$ close to the position of maximum velocity, exists in the flow field, so the value of α must be negative. For C-type flow, however, the value of α becomes positive, zero or negative, depending on the speed of the moving wall on which the maximum velocity exists. Moreover, a location where $\tau = 0$ does not exist in the flow field.

For P-type flow, the mean vorticity changes sign at the position of zero shear in the flow field of the channel as seen from the velocity profile, shown in figure 1(*a*). Accordingly we can assume mean negative and positive vorticities, respectively, in the upper and lower flow regions divided by the line $\tau = 0$, where the production of turbulent kinetic energy is zero. For C-type flow, on the other hand, the mean vorticity does not change sign throughout the flow field, so that we can assume a circulation, as shown in figure 1(*b*).

As the flow in the wall region is governed by the adjacent wall effect, similar treatment is possible in the near-wall region for both C- and P-type flows. In the turbulent core regions, however, there is an evident difference in the turbulence characteristic between the two flows, because the production of turbulent kinetic energy is not zero in the former, but is in the latter. Thus, we can conjecture that the similarity laws for the velocity profile and turbulence intensity differ greatly between P-and C-type flows. Therefore, different scaling for the velocity and length is needed in the turbulent core region for the P- and C-type flows.

For the law of the velocity profile and the turbulence structure, we divide the flow region into two parts, i.e. regions near the stationary and moving walls, at $y = h_s$, which divides the flow region for the P- and C-type flows. Here, h_s is the distance from the stationary wall to the dividing line. For P-type flow, h_s can be assumed to be δ_p. Since the distribution of shear stress is linear, the relations $h_s + h_m = 2h$ and

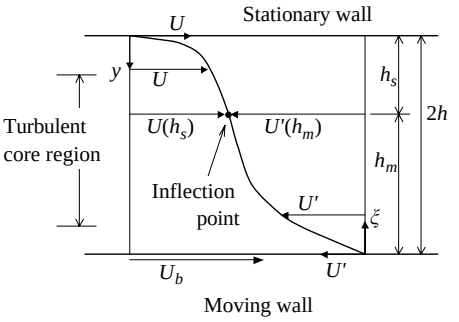

FIGURE 2. Galilean transformation for C-type flow ($\alpha > 0$).

$u_s^{*2}/u_m^{*2} = h_s/h_m$ hold. Here u_s^*, u_m^* and h_m are the friction velocities at the stationary and moving walls and the distance between the dividing line and the moving wall, respectively. So we can obtain

$$h_s = u_s^{*2}h/u_e^{*2} = u_s^{*2}h_m/u_m^{*2}, \tag{1}$$

where $u_e^* = \{(u_s^{*2} + u_m^{*2})/2\}^{1/2}$ is the effective velocity which differs by $1/\sqrt{2}$ from that defined by El Telbany & Reynolds (1980).

For C-type flow, however, there is no position where $\tau = 0$. Hence, different way to determine h_s is needed. Here, we assume that the flow region can be divided at the inflection point of the velocity profile, as shown in figure 1(*b*). Now we apply the following defect law in the flow region of the stationary wall:

$$[U(h_s) - U(y)]/u_s^* = D((h_s - y)/h_s)^n. \tag{2}$$

In the moving-wall region, we can assume that (2) will hold after applying the Galilean transformation, as shown in figure 2. A new coordinate, $\xi = 2h - y$, that is fixed on the moving wall, and $U' = U_b - U$ are used where U_b is the speed of the moving wall. Then $U(h_s) - U = U' - U'(h_m)$, $h_s - y = \xi - h_m$ are obtained. If $D = n = 1$ is assumed, the following relationship can be obtained:

$$[\{U'(h_s) - U'(y)\}/(h_s - y)]/[\{U'(h_m) - U'(\xi)\}/(h_m - \xi)] = (h_m/h_s)(u_s^*/u_m^*),$$

and therefore $h_m/h_s = u_m^*/u_s^*$

Hence, h_s is given by

$$h_s = 2hu_s^*/(u_s^* + u_m^*) = hu_s^*/\{(u_s^* + u_m^*)/2\} = hu_s^*/u_c^*, \tag{3}$$

where $u_c^* = (u_s^* + u_m^*)/2$.

In the turbulent core region, the flow-type parameter β is important. P- or C-type flow can be obtained for $\beta < -0.5$ or > -0.5, respectively. In particular, plane Poiseuille and Couette flows can be obtained for $\beta = -1$ and 0, respectively.

3. Experimental apparatus and method

Figure 3 shows a schematic view of the test channel, which is 5.4 m in length and 0.85 m in width. The upper wall is stationary and the lower wall, which consists of a flat belt, can be moved either with the air flow through the channel or in the opposite direction. The stationary-wall is made of acrylic plastic plate, while the moving wall is a polyester conveyer belt driven by a variable-speed motor. The channel depth $2h$ is 20, 40 or 80 mm depending on the experimental conditions being studied. The

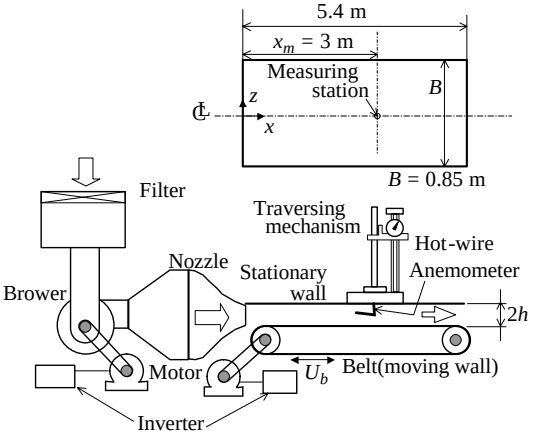

FIGURE 3. Experimental apparatus.

coordinates x, y and z are the streamwise distance from the channel inlet section, the wall-normal distance from the stationary-wall and the spanwise distance from the central plane of the channel, respectively. At the upstream end of the channel, a blower with a settling chamber and two-dimensional diffuser is attached to push air into the channel. By selecting various combinations of air flow rate and moving belt speed, we can obtain different kinds of C-P flow. Two motors to drive the blower and the belt were controlled by inverter units.

The belt speed U_b was measured optically by counting the number of tape strips passing through the sensor in a unit of time. The strips are glued on the edge of the belt at every 110 mm in the moving direction and reflect the emitted light from the sensor. The uncertainty in this measured speed is less than 1%. There were pressure holes on the stationary wall, every 200 mm in the x-direction, and the static pressure was measured at these points by a precision pressure cell (having 0.01 mmAq resolution).

The measurements of velocity were made at the central plane of the channel ($z = 0$) at the station $x_m = 3$ m from the inlet of the channel, where the flow was fully developed, as was confirmed by Nakabayashi *et al.* (1988). We measured mean velocity profiles and streamwise and wall-normal fluctuating velocity components (u and v) at the stationary-wall side by hot-wire anemometers with I- and X-type probes, respectively. The reliability of measurements was checked by comparison of Reynolds shear stress between the data measured directly by X-wire and the results estimated from the momentum balance equation given below using the mean velocity profiles.

Table 1 shows the symbols used in the following figures. The values of parameters in the table are based on the wall-stress scaling of the stationary-wall ($y = 0$) side for both P- and C-type flows. The Reynolds number Re^* of the present work covers fairly wide range, from very low to moderately high, but not the high-Re^* condition. These data sets are best suited for comparison with current DNS.

Figure 4 shows examples of normalized Reynolds shear stress distributions for various μ and β. Symbols show direct measurement data from the X-wire probe. Solid lines indicate the normalized Reynolds shear stress estimated from the momentum balance equation

$$-\overline{uv}^+ = 1 + y^+/\mu - \mathrm{d}U^+/\mathrm{d}y^+. \tag{4}$$

Poiseuille-type					Couette-type				
	μ	Re^*	$Re^{*\prime}$	β		μ	Re^*	$Re^{*\prime}$	β
●	−60	100	60	−1.66	⊠	−1334	105	109	−0.08
⊙	−127	96	127	−0.76	⊞	−464	112	130	−0.24
⊙	−137	164	137	−1.20	⧈	−413	175	252	−0.42
◑	−195	277	195	−1.42	■	35	156	75	4.48
◐	−216	455	216	−2.11	□	55	177	95	3.23
◓	−264	370	264	−1.40	▣	85	103	73	1.22
◒	−275	653	275	−2.37	◘	94	145	96	1.54
◎	−376	568	376	−1.51	◨	222	278	194	1.25
⊕	−383	421	383	−1.10	◧	258	99	85	0.38
⊗	−531	679	531	−1.28	⬒	451	160	139	0.35
					⬓	780	316	270	0.41
					⧗	902	100	95	0.11
					⧗	1333	159	151	0.12

TABLE 1. Parameters and symbols.

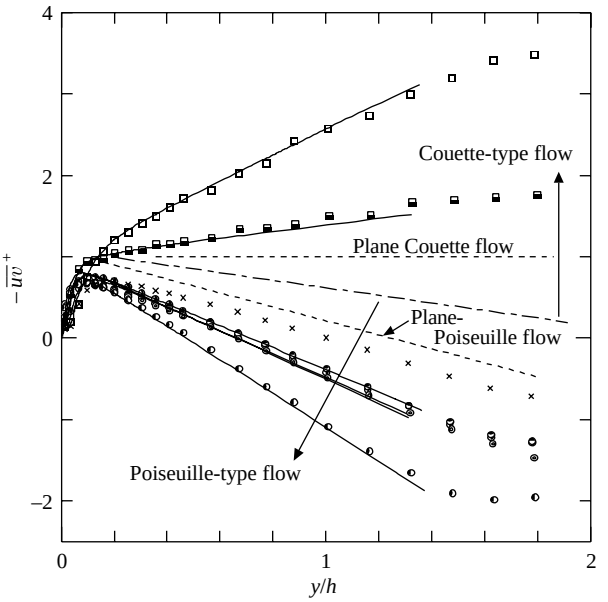

FIGURE 4. Reynolds shear stress distributions. For symbols, see table 1. ×, plane Poiseuille flow ($Re^* = 182$).

They agree very well. The chain line indicates the dividing line between C- and P-type flows. As $|\mu|$ decreases, the curve shifts upward or downward for positive or negative μ, respectively.

The result shows that the present data are reliable within an uncertainty of less than 1% for the mean velocity and about 4% for the Reynolds stress, except for the wall vicinity. The friction velocity u_s^* was estimated from the mean velocity profiles near the wall, based on the principle proposed by Bahtia, Durst & Jovanovic (1982) and the procedure used by Nagano *et al.* (1991).

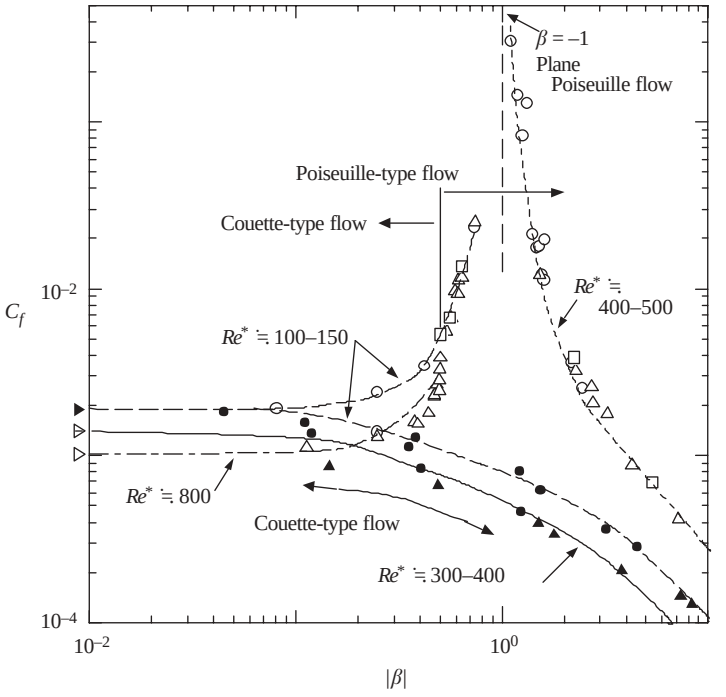

FIGURE 5. Wall-friction coefficient C_f. ○, $\alpha < 0$; ●, $\alpha > 0$, present results; △, $\alpha < 0$; ▲, $\alpha > 0$, El Telbany & Reynolds (1980); □, $\alpha < 0$, Kuroda & Kasagi (1993).

4. Wall-friction coefficient

Figure 5 shows the relationship between the viscous friction coefficient C_f non-dimensionalized by the belt speed $U_b[C_f = \tau_w/(\rho U_b^2/2)]$ and $\beta = \alpha h/u_s^{*2}$. Experimental results of El Telbany & Reynolds (1980) and DNS results of Kuroda *et al.* (1994) are also shown. Solid symbols in the figure are for $\alpha > 0$ and open ones for $\alpha < 0$. For $\alpha < 0$, C_f becomes infinite at $\beta = -1$ (plane Poiseuille flow), because $U_b = 0$ in the pure pressure flow. When β approaches infinity, C_f becomes zero, because the wall skin friction becomes zero. For $\alpha > 0$, when β approaches zero ($\alpha \to 0$: pure shearing flow, i.e. plane Couette flow), C_f approaches a maximum value which depends on Re^*. With increasing β, C_f decreases. Data scatter a little, because of the difference in Re^*. At the same value of β, C_f tends to slightly increase as Re^* decreases. In the figure, broken, solid, dot and chain lines indicate fitting curves of each data set for $Re^* \approx 100$–150, 300–400, 400–500, 800, respectively. The results described above agree with those obtained by El Telbany & Reynolds (1980) and Kuroda *et al.* (1994). The present experimental results for C_f for plane Couette flow, shown by triangles outside the left-hand verical axis, agree well with the following experimental formula given by Robertson (1959):

$$C_f = 2(0.095/\log(Re_b/4))^2. \tag{5}$$

Next we consider the relationship between the wall-friction coefficient C_f' scaled by the mean velocity $U(h_s)$ at the dividing line ($y = h_s$), i.e. $C_f' = \tau_w/(\rho U(h_s)^2/2))$, and $Re^{*\prime} = u_s^* h_s/\nu$. Here, $(C_f'/2)^{1/2}$ gives the ratio of the inner velocity scale u_s^* to the velocity $U(h_s)$. $Re^{*\prime}$ is the ratio of the distance from the dividing line to the stationary wall h_s to the viscous length scale $\delta_v = \nu/u_s^*$. Figure 6 shows a graph of C_f' against

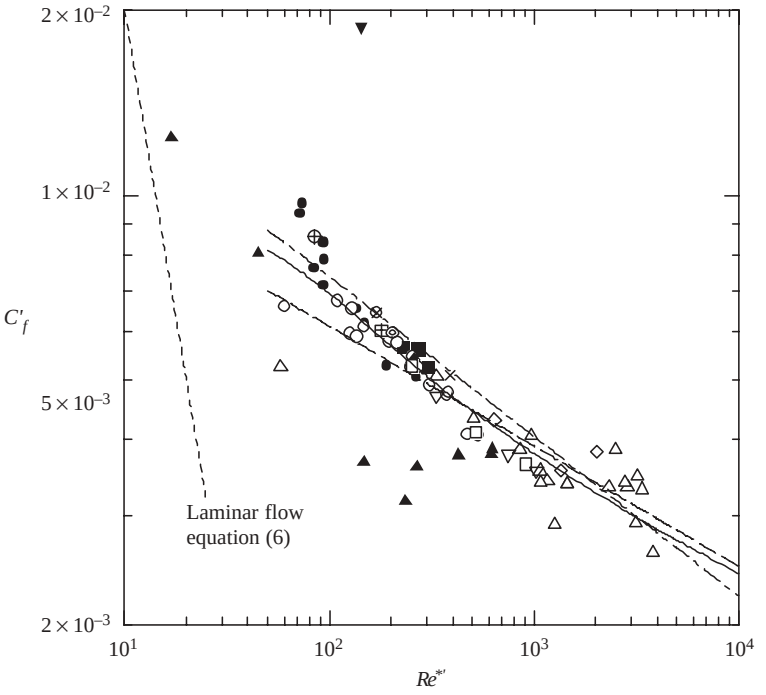

FIGURE 6. Wall-friction coefficient C'_f. For C-P flow: ○, $\alpha<0$; ●, $\alpha>0$, present results: △, $\alpha<0$; ▲, $\alpha>0$, El Telbany & Reynolds (1980): ■, $\alpha<0$ Kuroda & Kasagi (1993). For plane Couette flow: ◆, Nakabayashi *et al.* (1994): ⊕, Andersson *et al.* (1993): ⊗, Lee & Kim (1991). For plane Poiseuille flow: ◇, Hussain & Reynolds (1975): ▽, Johansson & Alfredsson (1982): ×, Kreplin & Eckelmann (1979): +, Kim *et al.* (1987): ◎, Nishino & Kasagi (1990): □, Antonia *et al.* (1992), ▼, Reichardt (1959). Solid line: Robertson (1959). Dot-dash line, Dean (1978). Broken line, Hussain & Reynolds (1975).

$Re^{*\prime}$ for the present results and the results of El Telbany & Reynolds for C-P flows, including those obtained by Kuroda *et al.* and other researchers for plane Poiseuille and Couette flows. In laminar flow, C'_f is the same for both plane Poiseuille and Couette flows, as given by

$$C'_f = 2/Re^{*\prime}. \tag{6}$$

In turbulent flow, C'_f for plane Couette flow is given by the Robertson formula, equation (5), shown by a solid line. For plane Poiseuille flow, on the other hand, the Hussain & Reynolds (1975) formula, which is shown by a broken line, is given by

$$u_s^*/U_c = 0.1079(Re_c/2) - 0.089, \tag{7}$$

where $U(h_s) = U_c$ and $Re_c = 2hU_c/\nu$. Dean's (1978) formula, indicated by a chain line, is given by

$$C_{fmean} = 0.073 Re_{mean}^{-1/4}, \tag{8}$$

where $C_{fmean} = 2u_s^{*2}/U_{mean}^2$ and $Re_{mean} = 2hU_{mean}/\nu$. U_{mean} is the bulk velocity averaged on the cross-section. The results of El Telbany & Reynolds show a large dispersion, and the result of Reichardt is too high. Except for the results of El Telbany & Reynolds and Reichardt, all other data including the present ones are nearly in agreement with the formulae given by equations (5), (7) and (8).

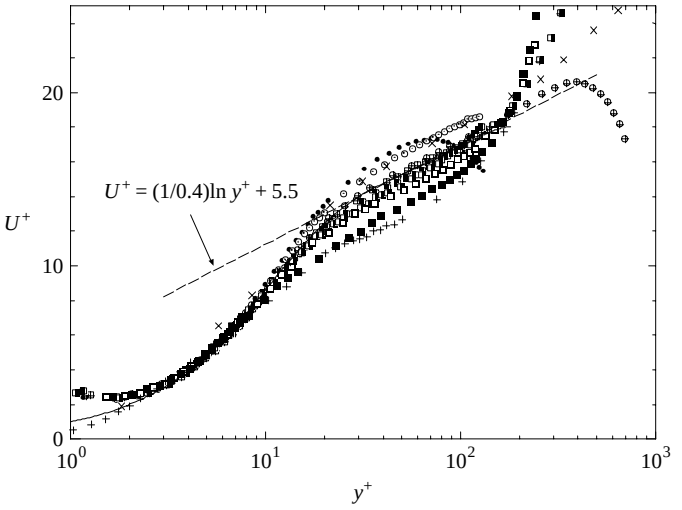

FIGURE 7. Mean velocity distributions normalized by inner scales. For symbols, see table 1. For boundary layer flow: ×, Blackwelder & Kovasznay (1972): +, Nagano *et al.* (1991). Solid line indicates DNS result obtained by Kim *et al.* (1987), $\mu = -180$, $Re^* = 180$.

5. Law of velocity distribution

5.1. *Law of the wall*

In the wall region, dimensional considerations allow us to write the velocity profile as the law of the wall as follows:

$$U^+ = F_1(y^+, \mu, Re^{*\prime}). \tag{9}$$

Here, $U^+ = U/u_s^*$, $y^+ = y/\delta_v = yu_s^*/\nu$, $\mu = \delta_p/\delta_v = u_s^{*3}/(|\alpha|\nu)$ and $Re^{*\prime} = u_s^* h_s/\nu$, where $\delta_p = u_s^{*2}/|\alpha|$ is the shear stress gradient length scale. When $Re^{*\prime}$ and μ are quite large, equation (9) reduces to

$$U^+ = F_1(y^+). \tag{10}$$

In the viscous sublayer, this reduces to

$$U^+ = y^+. \tag{11}$$

In the local equilibrium layer, where turbulent energy production equals energy dissipation, we can obtain the following log-law:

$$U^+ = 1/\kappa \ln y^+ + B, \tag{12}$$

where κ is the Kármán constant. The constants κ and B are generally dependent on $Re^{*\prime}$ and μ unless these parameters are quite large.

Figure 7 shows mean velocity distributions measured by the I-probe in a semi-log plot. The figure compares the DNS result for plane Poiseuille flow (Horiuchi 1993) and the experimental results of boundary layer flows with favourable (Blackwelder & Kovaszany 1972) and adverse pressure gradients (Nagano *et al.* 1991). Note that the definitions of μ and Reynolds number Re^* for the boundary layer flow are different from those for the C-P flows. For the boundary layer, α is the kinematic pressure gradient $\mathrm{d}p/\mathrm{d}x/\rho$ that is equal to the shear stress gradient $(\mathrm{d}\tau/\mathrm{d}y/\rho)_{wall}$ at the wall and the Reynolds number is defined by $Re^{*\prime} = u_s^*\theta/\nu$, where θ is the momentum thickness. In the neighbourhood of the wall, all data collapse onto a single curve. But in the

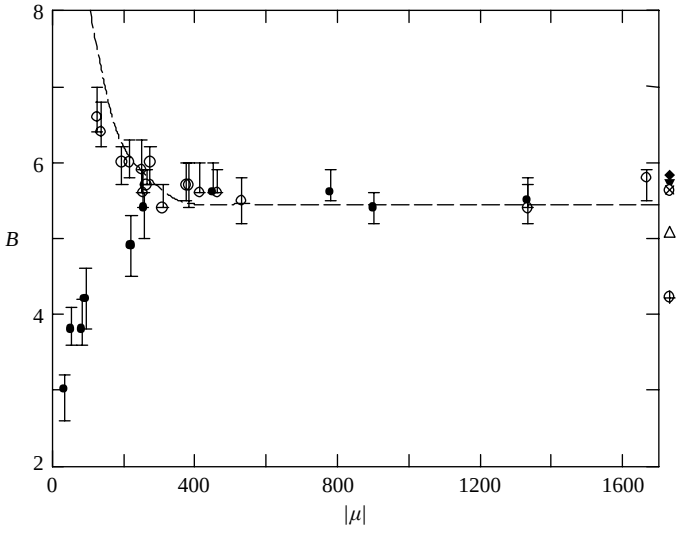

FIGURE 8. Additive constant B of the log law against $|\mu|$. ○, $\alpha < 0$; ●, $\alpha > 0$, present results. For plane Couette flow ($\mu = \infty$): △, $Re^* = 620$, El Telbany & Reynolds (1980): ◆, $Re^* = 260$, Nakabayashi *et al.* (1994): ⊕, $Re^* = 85$, Andersson *et al.* (1993): ⊗, $Re^* = 170$, Lee & Kim (1991). ▼, $Re^* = 143$, Reichardt (1959). Broken line, pipe flow, Patel & Head (1969).

region $y^+ > 10$, U^+ follows different curves depending on the values of $Re^{*\prime}$ and μ. For high values of $Re^{*\prime}$ and μ, the velocity distribution coincides with the conventional log-law (broken line); κ is considered to be a universal constant independent of $Re^{*\prime}$ and $|\mu|$. The existence of the log-law region at low Re^*, symbol ● in figure 8 for example, is not established but except for very low Re^* as here, most of the present data have a log-law region, Nakabayashi *et al.* (1988) and Nakabayashi, Kitoh & Nishimura (1997). As the absolute value of μ decreases, the velocity distribution shifts upward or downward in parallel for negative or positive value of μ respectively. The boundary layer flows with adverse and favourable pressure gradients show the same trend as the C-P flows with positive and negative μ, respectively.

Figure 8 shows the relation between B and the absolute value of μ. In the range $|\mu| > 400$, B takes a constant value of 5.5, although its values for plane Couette flow ($\mu = \infty$) shown by the symbols outside of the axis on the right in the figure have a large dispersion. With a decrease in absolute μ, however, B increases for negative μ and decreases for positive μ. For pipe flow, Patel & Head (1969) attributed this increase of B to the 'low Reynolds number effect'. But this attribution is not correct for other C-P flows except for plane Poiseuille flow. When the data are replotted against $Re^{*\prime}$, they cannot be arranged like figure 8 and show no systematic trend. We can say that B depends only approximately on μ. Accordingly, we may conclude that the 'low Reynolds number effect' may be attributed to the μ effect.

Figure 9 shows the relation between the Van-Driest damping coefficient A^+ and $|\mu|$. The Van-Driest model can be written

$$U^+ = \int_0^{y^+} 2/\left[1 + [1 + 4(\kappa y^+)^2\{1 - \exp(-y^+/A^+)\}^2]^{1/2}\right] \mathrm{d}y^+. \tag{13}$$

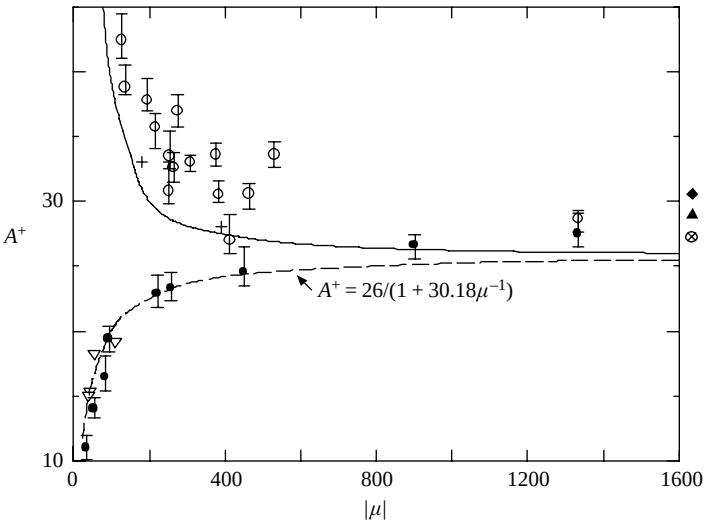

FIGURE 9. Van-Driest damping factor A^+. ○, $\alpha < 0$; ●, $\alpha > 0$, Present results. ▽, Boundary layer flow, Nagano *et al.* (1991). +, Plane Poiseuille flow, Antonia, *et al.* (1992). For plane Couette flow ($\mu = \infty$): ▲, El Telbany & Reynolds (1980): ◆, Nakabayashi *et al.* (1994): ⊗, Lee & Kim (1991). Solid line, plane Poiseuille flow, Huffman & Bradshaw (1972). Broken line, boundary layer flow, Kays (1971).

Lines indicate the results obtained by Huffman & Bradshaw (1972) for plane Poiseuille flows ($\mu < 0$) and those obtained by Kays (1971) for boundary layer flows with adverse pressure gradient ($\mu > 0$). The results of Antonia *et al.* (1992) for a plane Poiseuille flow and those of Nagano *et al.* (1991) for an adverse pressure gradient boundary layer are also shown. The present data agree well with these results. A^+ depends only on μ. When μ increases to infinity, A^+ approaches 26. As the absolute value of μ decreases, A^+ decreases for positive μ, but increases for negative μ. Thus both B and A^+ are affected very strongly by μ. Hence we show the relation between A^+ and B in figure 10. When $\mu \to \pm\infty$, $A^+ \to 26$ and $B \to 5.5$. For $\mu > 0$, B decreases with decreasing μ. But for $\mu < 0$, B increases with A^+ with decreasing $|\mu|$. A non-dimensional wall distance of $y^+ = A^+$ indicates a position related to the thickness of buffer layer. As shown later in figures 14 and 15, for $\mu > 0$, turbulent activity (turbulence intensity or turbulent kinetic energy production) becomes large at smaller y^+ with decreasing μ. Consequently, the buffer layer becomes thinner, as seen in figure 7, so that the value of A^+ becomes small and B decreases. For $\mu < 0$, on the other hand, an increase of A^+ means weaker turbulent activity with decreasing $|\mu|$, because the fully turbulent region moves far from the wall.

5.2. *Half-power law*

In a region somewhat further from the wall, it is possible that the shear stress gradient α is dominant, while the wall shear stress τ_w and distant wall h have little influence. Using α and u_s^* as independent dimensions, equation (9) can be written

$$U^+ = f_4\{y/\delta_p, \delta_v/\delta_p, h_s/\delta_p\}. \tag{14}$$

If we can assume the mixing length theory holds and a linear shear stress distribution, the following half-power law can be obtained:

$$U^+ = K_1\left(\alpha y/u_s^{*2}\right)^{1/2} + K_2 \tag{15}$$

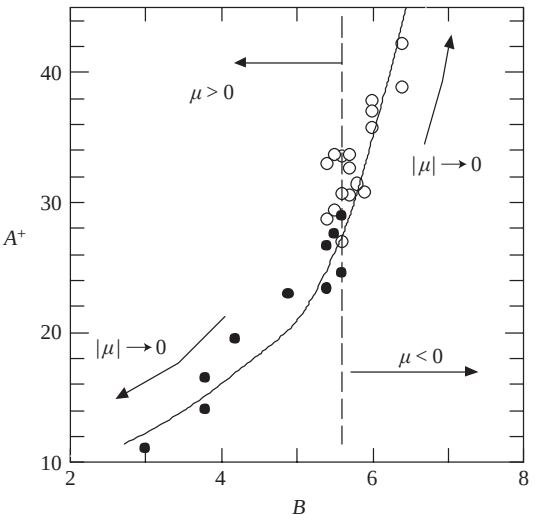

FIGURE 10. Relation between A^+ and B. ○, $\alpha < 0$; ●, $\alpha > 0$.

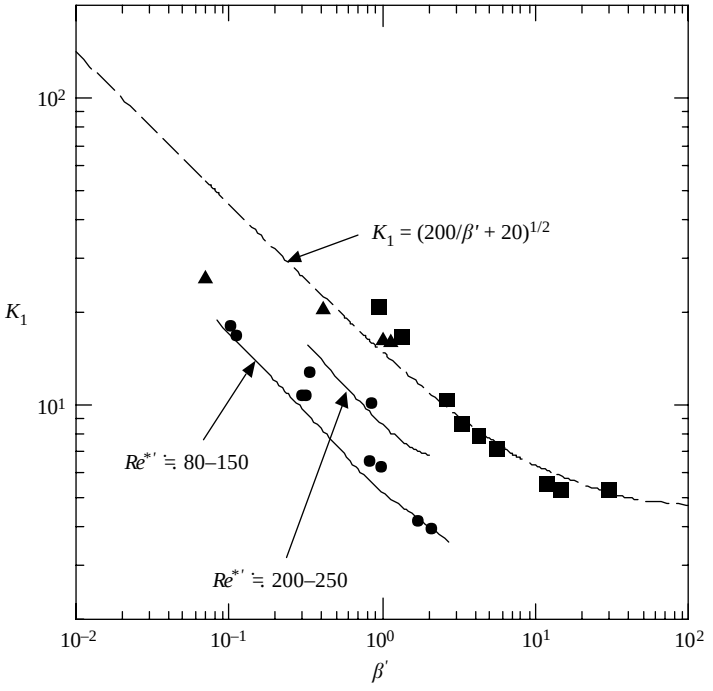

FIGURE 11. Coefficient of 1/2-power law K_1. ●, present results. ▲, El Telbany & Reynolds (1980); ■, Samuel & Joubert (1974). Broken line, Kader & Yaglom (1978).

K_1 and K_2 are constant. The half-power law holds just above the log-law region only for a flow with positive shear stress gradient ($\alpha > 0$). Figure 11 shows the relation between K_1 and flow parameter $\beta' = \alpha h_s / u_s^*$. The results by El Telbany & Reynolds (1980) for C-P flows, as well as the results of Samuel & Joubert (1974) and Kader & Yaglom (1978) for boundary layer flows are also shown. Solid circles indicate the present results and show a Reynolds number dependence that has not previously

	P-type	C-type
Characteristic velocity	u_e^*	u_c^*
Characteristic length	δ_p (stationary wall side)	h
h_s	$\dfrac{2hu_s^{*2}}{u_s^{*2}+u_m^{*2}}$	$\dfrac{2hu_s^*}{u_s^*+u_m^*}$

TABLE 2. Characteristic velocity and length scales and distance from the stationary wall to the line of division of the flow h_s: $u_e^* = (u_s^{*2}+u_m^{*2}/2)^{1/2}$, $u_c^* = (u_s^*+u_m^*)/2$, $\delta_p = u_s^{*2}/|\alpha| = 2hu_s^{*2}/(u_s^{*2}+u_m^{*2})$.

been pointed out. Solid curves indicate the results for which $Re^{*\prime}$ has approximately constant values. These curves indicate a tendency for the values of K_1 to decrease with increasing β', parallel to the result obtained by Kader & Yaglom. As the results of Samuel & Joubert are for high Reynolds number at $Re^{*\prime} = 2000$–3000, the curve given in Kader & Yaglom may show the limit for $Re^{*\prime} \to \infty$. As the reason why the present results have smaller values than the results for the boundary layer, we can conjecture that the shear stress gradient is not constant in the boundary layer and that Reynolds numbers $Re^{*\prime}$ of data are smaller for C-P flows than for the boundary layer flows.

5.3. *Defect law*

In the turbulent core region, the following defect laws are well known for plane Poiseuille and Couette flows, respectively:

$$[U(y=h)-U]/u_s^* = (1/2)R_s(1-y/h)^2 \quad \text{for plane Poiseuille flow.}$$
$$[U(y=h)-U]/u_s^* = R_s(1-y/h) \quad \text{for plane Couette flow.}$$

Here, $U(y=h)$ gives the maximum velocity for plane Poiseuille flow and the velocity at an inflection point of the profile for plane Couette flow, as seen in figures 1(*a*) and 1(*b*), respectively. The value of $R_s = u_s^* h_s/\varepsilon_T$, which incorporates the constant eddy viscosity ε_T, generally varies with Reynolds number $Re^{*\prime}$. For plane Couette flow, in particular, it varies from 3 to 5.8 with an increase of u_s^*/U_b from 30 to 47 (Nakabayashi *et al.* 1997).

For the case of C-P flows, distributions of mean velocity and shear stress vary largely according to the difference in turbulence characteristics between P- and C-type flows, as described later. Therefore it is necessary to change the characteristic velocity and length scales appropriately for P- and C-type flows. Based on the considerations in § 2 and the present experimental data, we propose the following formula for the defect law as a function of the distance y from the point of zero shear stress or the inflection point for P- or C-type flow using the respective characteristic velocity or length scale:

$$[U(h_s)-U(y)]/[\text{characteristic velocity}] = D[(h_s-y)/(\text{characteristic length})]^n. \quad (16)$$

Here, the characteristic velocity and length scales and h_s are given in table 2, where $u_e^* = [(u_s^{*2}+u_m^{*2})/2]^{1/2}$, $u_c^* = (u_s^*+u_m^*)/2$ and $\delta_p = u_s^{*2}/|\alpha| = (2hu_s^{*2})/(u_s^{*2}+u_m^{*2})$. The channel half-height h instead of h_s is designated the length scale for C-type flow, unlike the discussion developed in § 2, because this fits better with experimental results. Note that the present definitions of velocity and length scales differ from those of El Telbany & Reynolds, and that the effective friction velocity u_e^* is also defined differently.

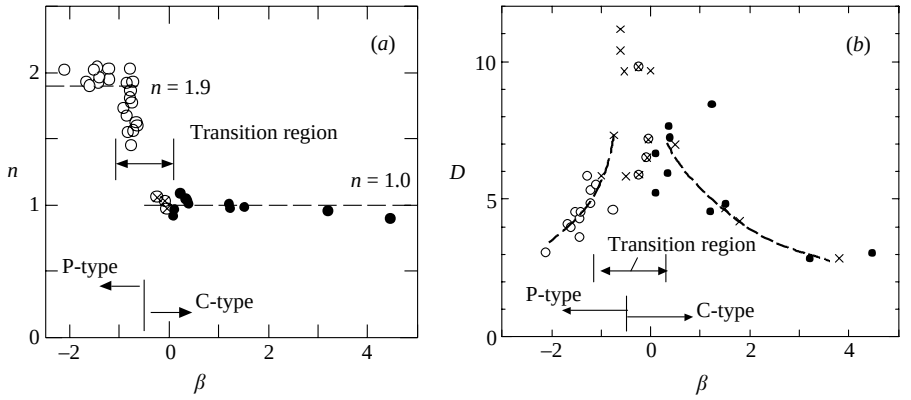

FIGURE 12. Constants of the velocity defect law. (*a*) Exponent n, (*b*) coefficient D. ○, $\alpha < 0$, P-type flow; ⊗, $\alpha < 0$, C-type flow; ●, $\alpha > 0$, C-type flow; present results. ×, El Telbany & Reynolds (1980).

Figure 12 shows exponent n and coefficient D in equation (16) against β, where $\beta < -0.5$ and $\beta > -0.5$ belong to P-and C-type flow, respectively; $\beta = -1$ is plane Poiseuille flow; $\beta = 0$ indicates plane Couette flow. The present results for n are approximately the same as those of El Telbany & Reynolds who obtained $n = 1.9$ for P-type flow and $n = 1.0$ for C-type flow. The present value of n varies from about 2.0 to 1.0 in the transition region ($\beta = -1.1$–0.3), where the flow varies from P-type to C-type. The present study gives a different result for the coefficient D from that of El Telbany & Reynolds, because their formula for the defect law differs from ours. When we apply equation (16) as the defect law to their data, their result agrees very well with the present result, as shown in figure 12(*b*). However, both data sets disperse widely in the transition region of β where the type of flow changes from P-type to C-type. Except for the transition region, however, both data decrease with increasing $|\beta|$.

The eddy viscosity ε_T is given by

$$\varepsilon_T = \left[u_s^{*2}\{1 + y/\delta_p \operatorname{sgn}(\alpha)\} - \nu \, \mathrm{d}U/\mathrm{d}y\right]/(\mathrm{d}U/\mathrm{d}y). \tag{17}$$

The dimensionless eddy viscosity $\varepsilon_T/(u_s^* h)$, which is the inverse of the turbulent Reynolds number, gives $2/R_s$ for plane Poiseuille flow and $1/R_s$ for plane Couette flow, respectively. For C- P flows, however, velocity and length scales have to change, as described above (table 2). In the turbulent core region ε_T takes its maximum (nearly constant) value and the dimensionless eddy viscosity is plotted in figure 13. In the transition region, it changes linearly with β but tends to have a rather constant value outside the transition region.

6. Turbulence characteristics

No definite discussion has been given so far on the similarity laws of the turbulence intensities. First, we summarize the relations obtained by dimensional analysis before considering them on the basis of the present experimental results. In the stationary-wall region, the following equation can be written:

$$u'/u_s^* = u'^{+} = f_1(y^+, \mu, Re^{*\prime}), \tag{18}$$

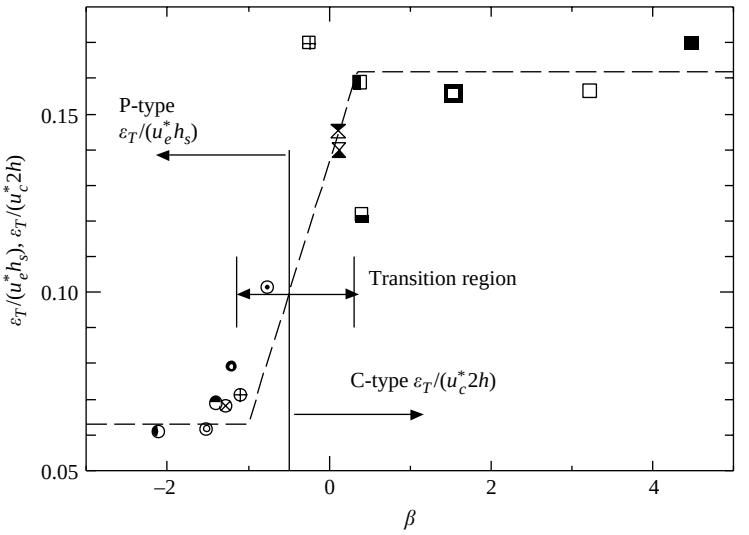

FIGURE 13. Relation between maximum values of kinematic eddy viscosities and β. For symbols, see table 1.

where $u' = \overline{(u^2)}^{1/2}$. As described later, $Re^{*\prime}$ is less effective than μ, so u'^+ can also be written as

$$u'^+ = f_2(y^+, \mu). \tag{19}$$

As the wall is approached, this equation can be expanded in a Taylor series.

$$u'^+ = A_1(\mu) y^+ + A_2(\mu) y^{+2} + \cdots. \tag{20}$$

Very close to the wall, the higher-order terms are omitted and the following linear relation results:

$$u'^+ = A_1(\mu) y^+. \tag{21}$$

When the values of both y^+ and μ are large, the 'plateau' region appears:

$$u'^+ = B \tag{22}$$

A turbulent core region exists in the central part of the channel, where different velocity scales and coordinates should be taken depending on whether C- or P-type flow occurs, as described before. For P-type flow, a new coordinate η defined by $\eta(= y - h_s)$ and an effective friction velocity $u_e^*(=[(u_s^{*2} + u_m^{*2})/2]^{1/2})$ are preferred. For C-type flow, the velocity scale is scaled by $u_c^*(=(u_s^* + u_m^*)/2)$, as described before. Consequently, the following relations can be obtained:

$$u'/u_e^* = f_3(\eta/h, \beta), \tag{23}$$

for P-type flow;

$$u'/u_c^* = f_4(\eta/h, \beta), \tag{24}$$

for C-type flow.

6.1. *Turbulence intensities in the wall region*

Figure 14 shows the variation of u'^+ according to the wall-stress scaling of equation (18). Profiles for similar μ values but different $Re^{*\prime}$ value do not differ so much. The influence of Re^* is small, so equation (19) is adequate. For $y^+ < 6$, equation (21)

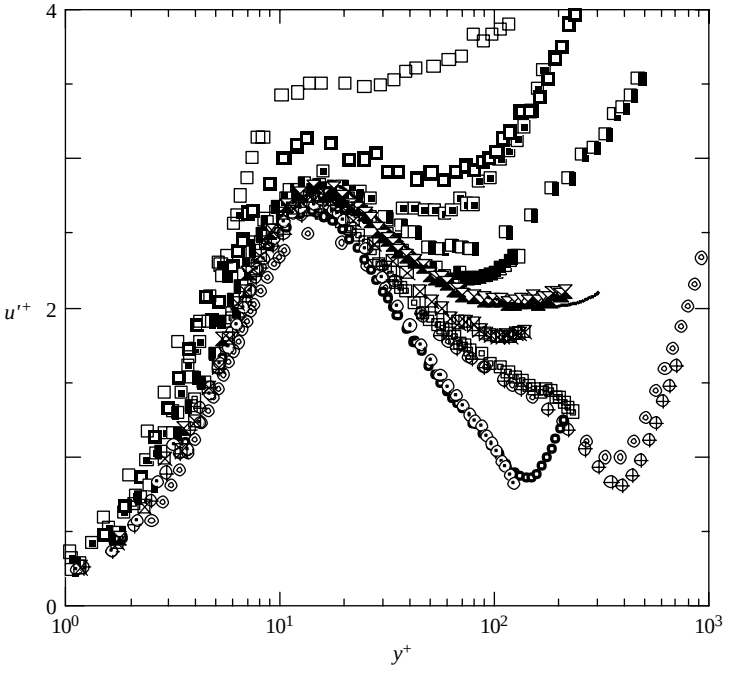

FIGURE 14. Turbulence intensity of u scaled by inner scaling. For symbols, see table 1. Solid line, plane Couette flow, Nakabayashi *et al.* (1997).

can be confirmed. When the values of both μ and y^+ are large, say $\mu = 1333$ and $y^+ = 80$–100, the 'plateau' region described later appears, where equation (22) holds. As $|\mu|$ decreases, the profile of u'^+ shifts upwards for $\mu > 0$ or downwards for $\mu < 0$ from the limiting value of u'^+ for $\mu = \pm\infty$, respectively. This tendency comes from the variation in turbulent kinetic energy production

$$\left(-\overline{uv}(\mathrm{d}U/\mathrm{d}y)\left(\nu/u_s^{*4}\right) = -\overline{uv}^+(\mathrm{d}U^+/\mathrm{d}y^+)\right)$$

with μ, as shown in figure 15. Here for $\mu > 0$, the dimensionless Reynolds shear stress $(-\overline{uv}^+)$ increases with μ^{-1}, while $\mathrm{d}U^+/\mathrm{d}y^+$ does not change much with μ. This assures a large production rate of turbulent kinetic energy for small positive μ. For $\mu < 0$, however, the location of $\tau = 0$, at which no production of the kinetic energy occurs, approaches the wall with increasing $|\mu|^{-1}$. Hence, as $|\mu|$ decreases, the turbulence intensity profile shifts downwards, as seen in figure 14. Since the relation $Re^{*\prime}(=Re^*) = -\mu$ holds in plane Poiseuille flow, it is natural to assume that the variation in turbulence intensities, the so-called 'low Reynolds number effect' for plane Poiseuille flow, is caused by the effect of the low μ value, as described in § 5.1.

Figure 16 shows coefficient A_1 of equation (21) against $|\mu|$. The value of $A_1(\mu)$ increases for $\mu > 0$ or decreases for $\mu < 0$ with decreasing $|\mu|$. The present results agree with the data of El Telbany & Reynolds and the cases of both plane Poiseuille and boundary layer flows. Accordingly, it is assumed that the asymptotic behaviours of near-wall turbulence are the same for both boundary layer and channel flows and depend only on μ.

Figure 17 shows the peak values of $u'^+(u'^+_{peak})$ and their location $(y^+_{u'peak})$ against $|\mu|$. The μ dependence of the peak value changes with the sign of μ, when $|\mu|$ becomes smaller than about 200. For negative μ, the peak value agrees with that of

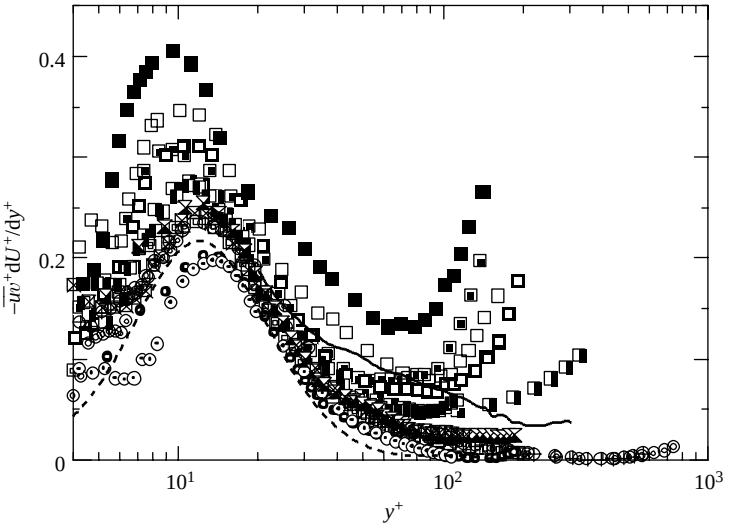

FIGURE 15. Production term of turbulence kinematic energy. For symbols, see table 1. Solid line, plane Couette flow, Nakabayashi *et al.* (1997), dashed line, plane Poiseuille flow, $Re^* = 180$, Horiuti (1993).

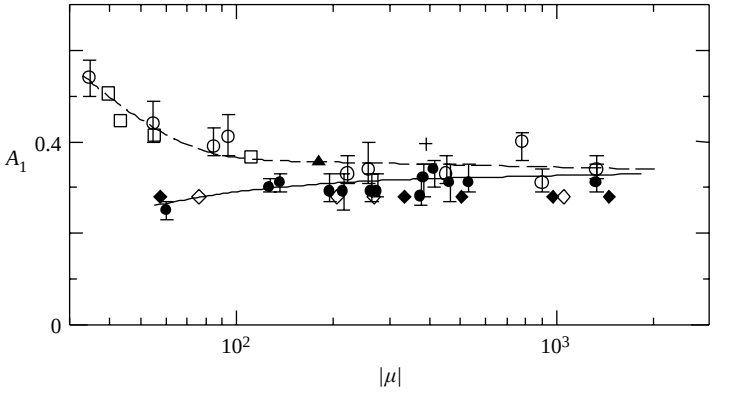

FIGURE 16. Coefficient A_1. ●, $\mu < 0$; ○, $\mu > 0$, present results. ◆, $\mu < 0$; ◇, $\mu > 0$, El Tebany & Reynolds (1981). For boundary layer flow: □, $\mu > 0$, Nagano *et al.* (1993). For plane Poiseuille flow: +, Antonia, *et al.* (1992): ▲, Kim *et al.* (1987).

plane Poiseuille flow. For positive μ, the peak value that differs slightly from that of boundary layer flow increases with decreasing μ. The relation between $|\mu|$ and the peak position has a similar tendency to that between $|\mu|$ and the peak value. As $|\mu|$ becomes smaller than about 200, the peak position increases with decreasing $|\mu|$ and becomes larger than that of the boundary layer flow with adverse pressure gradient. This suggests that the turbulence behaviour begins to differ, in the region beyond $y^+ \approx 15$, between turbulent channel and boundary layer flows for the smaller μ case, although the asymptotic behaviour of near-wall turbulence is similar in both flows.

The plateau region described above can be seen in the region $y^+ = 80$–100 for $\mu = 1333$ in figure 18. The results obtained by El Telbany & Reynolds (1981) in C-P flow and by Nakabayashi *et al.* (1997) in plane Couette flow are also shown. Following El Telbany & Reynolds, the plateau region exists for $y^+ > 80$ in the case

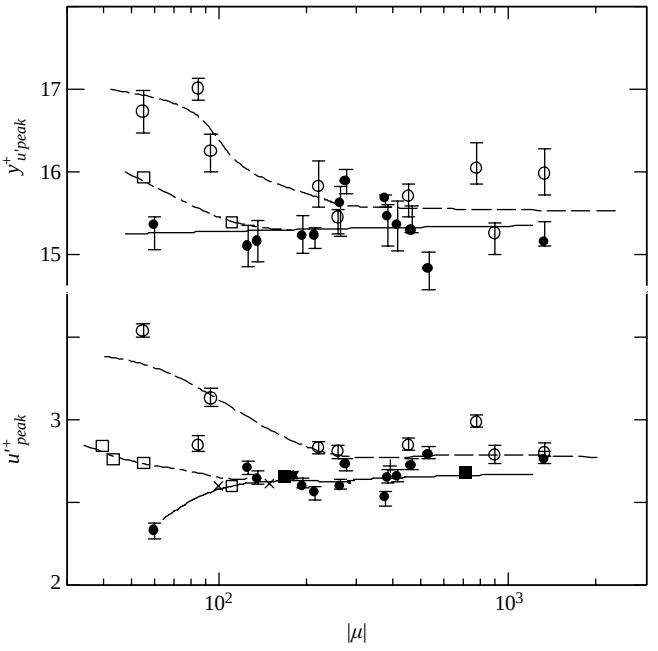

FIGURE 17. Peak value of u^+ and its location. ●, $\mu < 0$; ○, $\mu > 0$, present results. For boundary layer flow: □, $\mu > 0$, Nagano *et al.* (1993). For plane Poiseuille flow: +, Antonia *et al.* (1992): ▲, Kim *et al.* (1987): ▼, Horiuti (1993): ×, Kuroda (1990) ■, Wei & Willmarth (1989). Solid lines indicate the tendency of present data with $\mu < 0$. Broken lines indicate the trend of data with $\mu > 0$. Dot-dash lines indicate the trend of boundary layer data with $\mu > 0$.

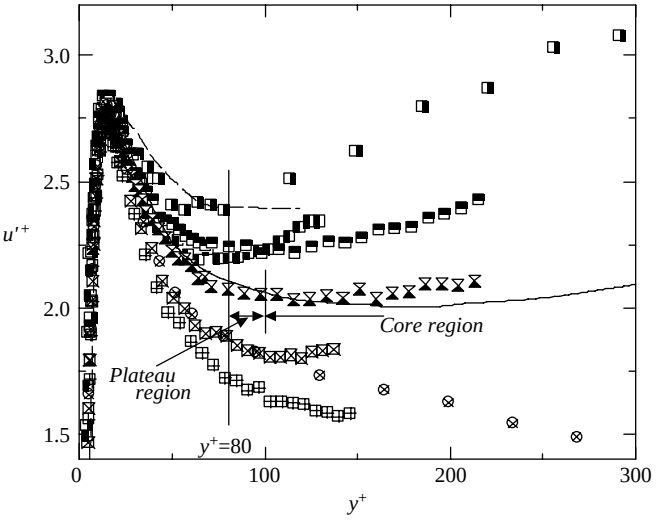

FIGURE 18. Plateau region of u^+. For symbols, see table 1. Solid line, plane Couette flow, Nakabayashi *et al.* (1997); broken line, El Telbany & Reynolds (1981).

of $|\mu| > 200$. In fully developed plane Poiseuille flow, however, Kitoh & Nakabayashi (1993) reported that the plateau region appeared for $y^+ > 80$ when $Re^* > 1500$. Since $Re^* = Re^{*\prime} = -\mu$ holds in plane Poiseuille flow and the influence of Reynolds number on the turbulence intensity is small in the wall region, the plateau region can be

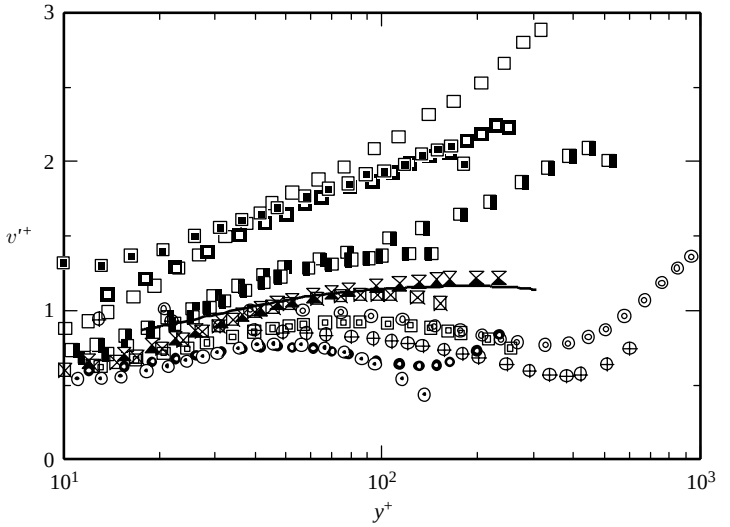

FIGURE 19. Turbulence intensity of v scaled by inner scaling. For symbols, see table 1. Solid line, plane Couette flow, Nakabayashi *et al.* (1997).

conjectured to appear for the condition $|\mu| > 1500$. The cases of $\mu = 1333$ and -1334 are the largest values of μ in the present experiment. The distribution of u'^+ at $\mu = 1333$ is close to that for plane Couette flow, and the plateau region exists just below the core region estimated from the mean velocity profile. Hence we can assume the existence of a plateau region for $\mu = 1333$. In the profile at $\mu = -1334$, however, one cannot be sure that the plateau region exists, because the profile of u'^+ at $\mu = -1334$ is too low compared with that for the plane Couette flow, and the dependence on y^+ appears on the profile.

Figure 19 shows the turbulence intensity of the wall-normal component in the wall region for P-type flow, plotted according to the wall-stress scaling. Here we consider only reliable data, i.e. data obtained at $y^+ > 40$. As the absolute value of μ decreases, the profile shifts upwards from that of $\mu = \infty$ for positive μ, but downwards for negative μ. This tendency is similar to the streamwise component u'^+.

6.2. *Turbulence intensities in the turbulent core-region*

Figure 20(a) shows distributions of turbulence intensity u' in the turbulent core region scaled by u_e^* according to equation (23) for P- type flow. The results obtained by El Telbany & Reynolds (1981) are higher and more widely scattered than the present results, which are distributed along a curve for plane Poiseuille flow. The profile generally shifts upwards with decreasing β, so the value of u'/u_e^* at $\eta = 0$ increases with decreasing β. In the plane Poiseuille flow, that is a special case of C-P flow, the position of the minimum value of u'/u_e^* located at the centre of the channel agrees with the positions of both zero Reynolds shear stress and maximum velocity. However, they generally do not coincide with each other in C-P flow. Now, let y_1, y_2 and y_3 be the positions of the maximum velocity where viscous shear stress is zero, the position of zero Reynolds shear stress and the position of the minimum value of u'/u_e^*, respectively. We shall define the difference in their positions from the position of zero total shear stress $y = \delta_p$ as $\Delta y_i = y_i - \delta_p (i = 1, 2 \text{ and } 3)$. Figure 20($b$) shows the relation between $\Delta y_i/h$ and β. The position of maximum velocity shifts to the high-shear-stress wall side as β decreases for $\beta < -1$ (i.e. $\Delta y_1 > 0$). But the position

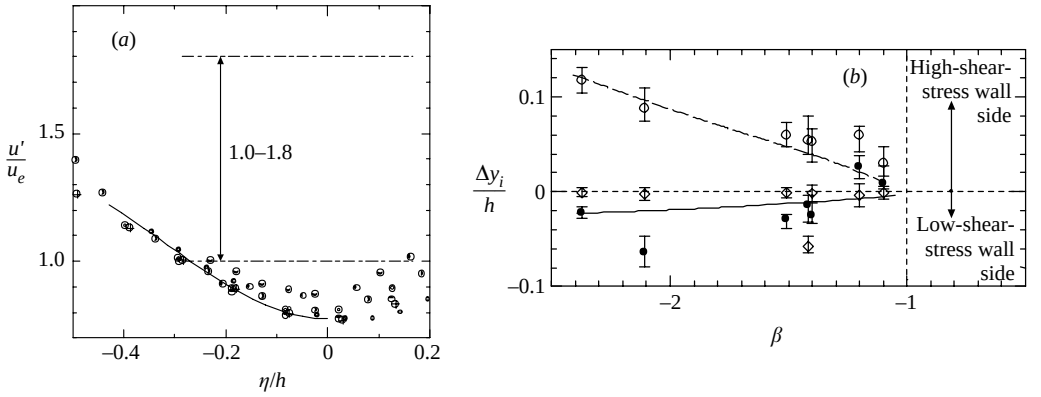

FIGURE 20. Turbulence intensity of u in the core region for P-type flow. (a) Turbulence intensity of core region. For symbols, see table 1. Solid line, plane Poiseuille flow, Horiuti (1993). (1.0–1.8) shows the range of data obtained by El Telbany & Reynolds (1981). (b) $\Delta y/h$. ○, $i=1$ (y_1 is the position of $U_{max.}$); ◇, $i=2$ (y_2 is the position of $\overline{uv}=0$) ●, $i=3$ (y_3 is the position of $(u'/u_e^*)_{min}$).

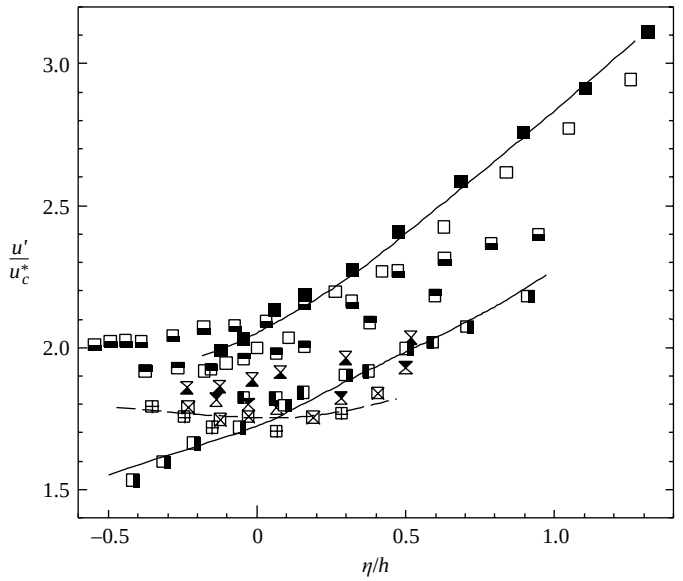

FIGURE 21. Turbulence intensity of u in the core region for C-type flow. For symbols, see table 1.

of zero Reynolds shear stress does not vary (i.e. $\Delta y_2 \approx 0$). On the other hand, the position of the minimum value of u'/u_e^* tends to shift to the low-shear-stress wall side (i.e. $\Delta y_3 < 0$). Here, the high- or low-shear-stress side means the wall side having higher or lower absolute wall shear stress than the other, respectively.

In the turbulent core region for C-type flow, the distribution of turbulence intensity u' scaled by u_c^* is shown according to equation (24) in figure 21. The profile, which shifts upwards with increasing β, has a tendency to increase with η/h for $\beta > 0$, but has a minimum value around $\eta = 0$ for $\beta < 0$.

Figure 22 shows relative turbulence intensity of the wall-normal component v' in the turbulent core region for P-type flow. The present results are distributed around

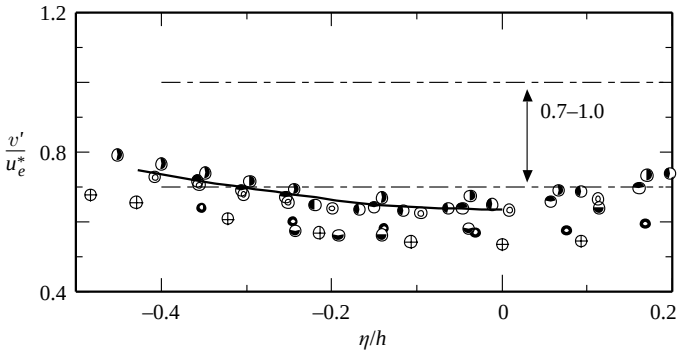

FIGURE 22. Turbulence intensity of v in the core region for P-type flow. For symbols, see table 1. Solid line, plane Poiseuille flow, Horiuti (1993). (0.7–1.0) shows the range of data obtained by El Telbany & Reynolds (1981).

the DNS result obtained by Horiuti (1993) for plane Poiseuille flow and show a slight increase with decreasing β. For reasons to be discussed in the following subsection with regard to the shear correlation coefficient, El Telbany & Reynolds' results are higher than the present results. The wider dispersion of their data comes from the wider range of $\beta(-7.2 < \beta < -1.0)$ than the present experiment.

6.3. *Shear correlation coefficient*

Figure 23 shows variation in the shear correlation coefficient with y/h for P-type flow. Although the peak in the near-wall region given by DNS result cannot be seen in the present experimental results, the measurements gave reasonable results except for the near-wall region. With increasing β, the zero shear correlation coefficient moves away from the wall, because it is given by the relation $y = \delta_p = |\beta|h$.

Figure 24 shows the shear correlation coefficient for C-type flow. Note that this flow has no zero-correlation point in the flow region. Except for the near-wall region, i.e. $y/h > 0.4$, the correlation coefficient has a value of about 0.45 at its maximum, which is typical of turbulent uniform shear flow, as reported by Tavoularis & Karnik (1989). El Telbany & Reynolds (1981) reported a much larger value of 0.7–0.75 for C-type flow as shown by the chain line in figure 24(*a*). The section measured in their experiment was $(45–20) \times (2h)$ from the inlet section. Compared to the $(150–37) \times (2h)$ in our experiment, this was too short to obtain turbulent statistics for fully developed flows. Figure 24(*b*) shows the correlation coefficients at $y/h = 1$ and 0.6 against β. The correlation coefficient decreases and approaches an asymptotic value as β increases. However, the data are a little scattered by the change in Re^* around $\beta \approx 0$.

6.4. *Skewness factor*

Figure 25 shows distribution of the skewness factor for the u-component $S(u)$ against y^+ for various μ and $Re^{*\prime}$. The solid and dotted lines indicate the experimental results for plane Couette flow ($\mu = \infty$, $Re^{*\prime} = 253$, Nakabayashi *et al.* 1997) and DNS for plane Poiseuille flow ($Re^{*\prime} = 180$, Horiuti 1993), respectively. In the wall region, results for $S(u)$ with nearly the same μ but different $Re^{*\prime}$ (e.g. those for row 8 on the left and row 3 on the right in table 1, as shown in the figure) are almost the same, indicating that $Re^{*\prime}$ does not have the appreciable effect on the $S(u)$ profile that μ does. Thus $Re^{*\prime}$-independence is similar to the turbulence intensity profiles described in § 6.2. In general, $S(u)$ increases (when $\mu > 0$) or decreases (when $\mu < 0$) from the value of $\mu = \infty$ (plane Couette flow) as $|\mu|$ decreases. For $\mu > 0$, the upward deviation of each

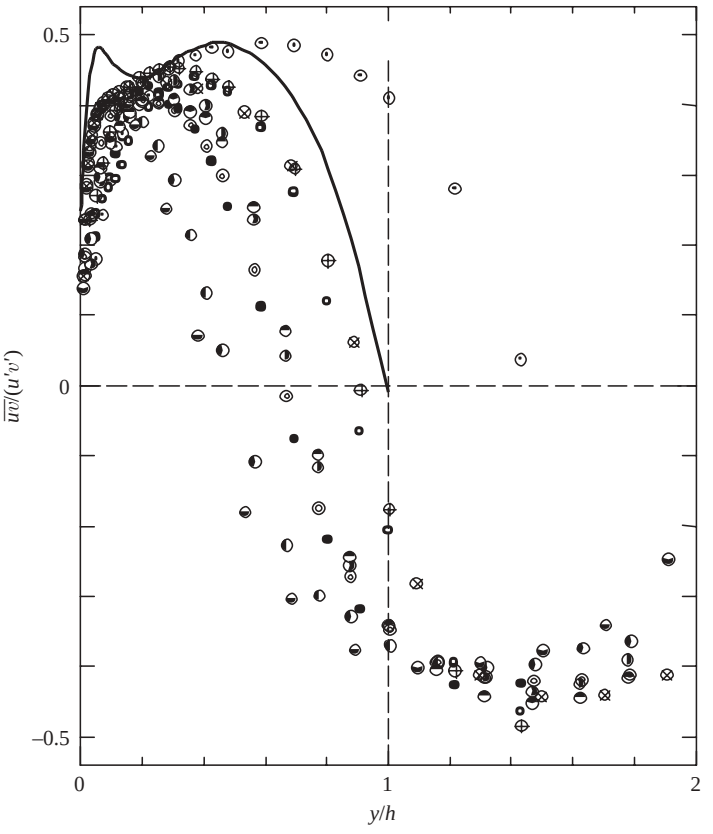

FIGURE 23. Shear correlation coefficient of P-type flow. For symbols, see table 1. Solid line, plane Poiseuille flow, Horiuti (1993).

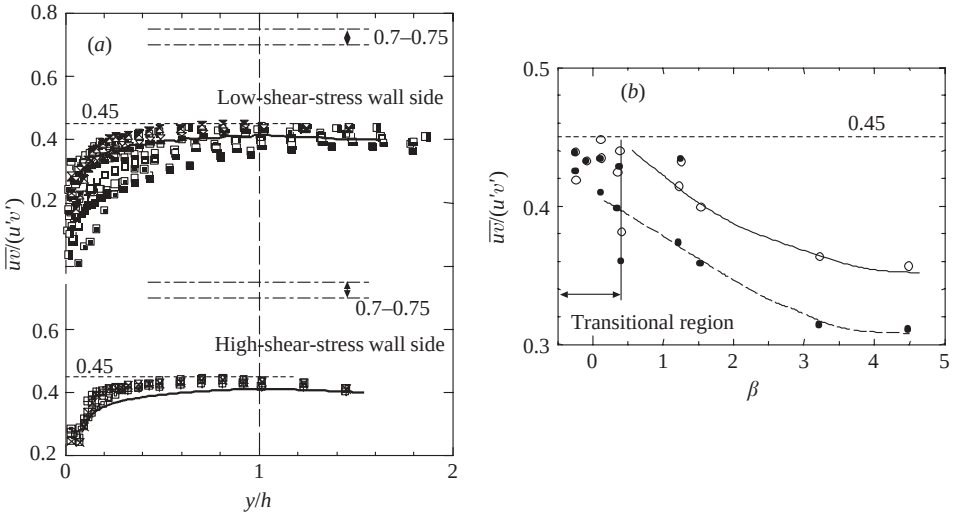

FIGURE 24. Shear correlation coefficient of C-type flow. (*a*) Distribution. Solid line, plane Couette flow, Nakabayashi *et al.* (1997). (0.7–0.75), shows the range of data obtained by El Telbany & Reynolds (1981). (*b*) Shear correlation coefficient at constant y/h against β. ● and broken line, $y/h = 0.6$; ○ and solid line, $y/h = 1.0$. Dotted line and (0.45) indicate data on turbulent uniform shear flow by Tavoularis & Karnik (1989).

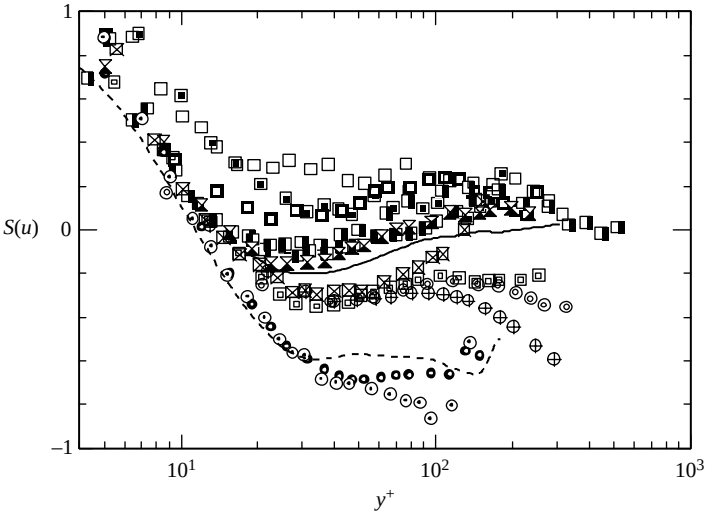

FIGURE 25. Skewness factor of u. For symbols, see table 1. Dotted line, plane Poiseuille flow, Horiuti (1993). Solid line, plane Couette flow, Nakabayashi *et al.* (1997).

profile from that of $\mu = \infty$ is more significant as the wall is approached. This can be explained as follows. As shown in figure 14, the turbulent motion becomes more and more active in the region away from the wall as $\mu(>0)$ decreases and the high velocity there penetrates inside the near-wall region so as to cause a strong sweep event. This is the reason for the noticeable increase in $S(u)$ near the wall for $\mu > 0$. In particular, as μ decreases below 94, negative $S(u)$ disappears from the channel section because the intensified sweep contributes more to the Reynolds shear stress than the ejection, as shown in the next section. For $\mu < 0$, however, $S(u)$ shifts downward from $\mu = \infty$ in the region away from the wall for the following reasons. In the case of $\mu < 0$, the turbulence intensity and/or the turbulent kinetic energy production in the outer wall region become more and more weak compared with that in the buffer region as $|\mu|$ decreases. The ejection of low-speed fluid into the outer wall region overwhelms the sweep, as described in the next section. In the region of y^+ less than about 10, however, negative μ has no effect on $S(u)$ at all, so the ejection and the sweep events are presumably unaltered.

6.5. *Four-quadrant analysis of fluctuating velocities*

Frequencies and fractional contributions to the Reynolds shear stress from each velocity quadrant are studied by a four-quadrant analysis. Figure 26 gives a typical example of P-type flow ($\mu = -195$, $Re^* = 277$). Here, $(-\overline{uv})_i$ is the contribution to the Reynolds shear stress from the i-quadrant. In figure 26(a), the correspondence between the types of events (ejection, sweep and interaction) and each quadrant is shown. Variations in the fractional contribution and frequency against y/h for P-type flow are similar to those of plane Poiseuille flow, i.e. the contribution from the ejection with small frequency is larger than that from the sweep on either of the walls. Figure 27 shows an example of the fractional contribution of C-type flow with large positive shear stress gradient ($\mu = 35$, $Re^* = 156$). Unlike P-type flow, the sweep contributes more to the Reynolds shear stress than ejection.

The effect of shear stress gradient on the fractional contribution is different between P- and C-type flows. To determine the effect, the relative fractional contribution

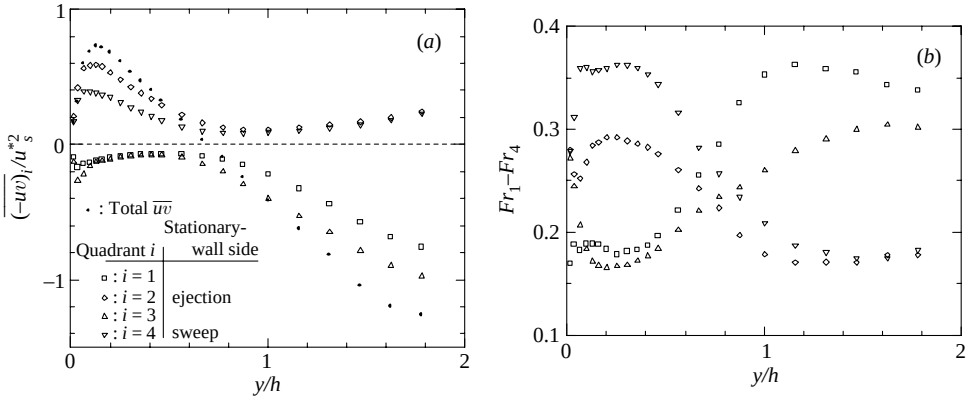

FIGURE 26. Example of four-quadrant analysis for P-type flow ($Re^* = 277$, $\mu = -195$). (*a*) Fractional contribution, (*b*) frequency. ●, total ($\overline{uv}$), □, quadrant 1 (sweep event on moving-wall side); ◇, quadrant 2 (ejection event on stationary-wall side); △, quadrant 3 (ejection event on moving-wall side); △, quadrant 4 (sweep event on stationary-wall side).

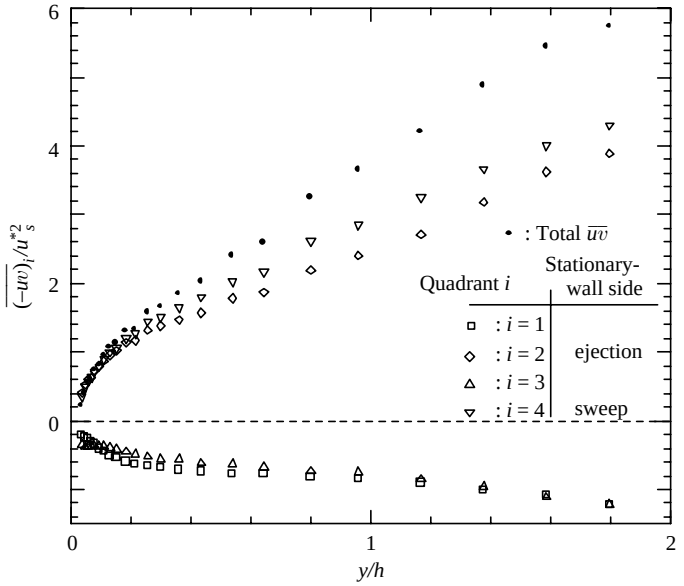

FIGURE 27. Example of fractional contribution by four-quadrant analysis for C-type flow ($Re^* = 156$, $\mu = 35$). ●, Total ($\overline{uv}$), □, quadrant 1 (sweep event on moving-wall side); ◇, quadrant 2 (ejection event on stationary-wall side and sweep event on moving-wall side); △, quadrant 3 (ejection event on the moving-wall side); ▽, quadrant 4 (sweep event on stationary-wall side and ejection event on moving-wall side).

defined as $(-\overline{uv})_4/(-\overline{uv})$ is plotted against y^+ for various μ in figure 28 for C-type flow. The relative fractional contribution from quadrant-4 increases near the wall ($y^+ < 100$–200) as positive μ decreases. Thus, the contribution from a sweep becomes stronger as μ decreases and, finally when μ decreases below around 50, the sweep prevails over the ejection. This is a peculiar feature of C-type turbulence with a large positive shear stress gradient.

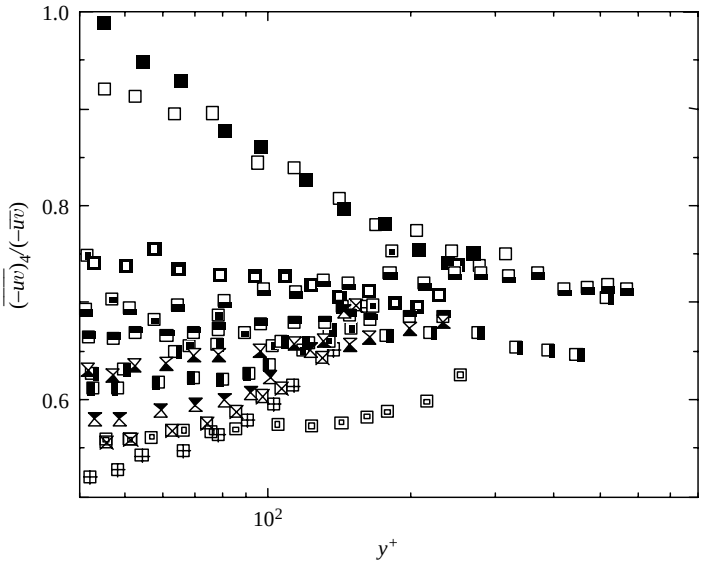

FIGURE 28. Relative fractional contribution from quadrant 4 for C-type flow. For symbols, see table 1.

7. Conclusions

Similarity laws for mean velocity profiles and turbulence characteristics of C-P turbulent flow have been studied. The global parameters of C-P flow are Reynolds number $Re^* = u_s^* h/\nu$ and the dimensionless shear stress gradient $\mu = u_s^{*3}/(\alpha\nu)$ or flow parameter $\beta = \alpha h/u_s^{*2}$, where $\alpha = \mathrm{d}(\tau/\rho)/\mathrm{d}y$. Re^* and $|\mu|$ values covered in this work are $96 \leqslant Re^* \leqslant 679$ and $35 \leqslant |\mu| \leqslant 1334$, respectively. The flow field is divided into two regions, say upper and lower regions, at $y = h_s$, i.e. at $\tau = 0$ for P-type flow or at an inflection point of the velocity profile for C-type flow. Various length and velocity scales appear in C-P flow. Depending on the flow type and flow region considered, the appropriate length and velocity scales are adopted for similarity laws. The main conclusions obtained are as follows.

(i) The wall friction coefficient scaled by belt speed, $C_f = \tau_w/(\rho U_b^2/2)$, is given as a function of both Reynolds number Re^* and flow parameter β. But the wall friction coefficient scaled by the mean velocity at the dividing line of the flow ($y = h_s$), $C_f' = \tau_w/(\rho U(h_s)^2/2)$, is given only by the parameter $Re^{*\prime} = u_s^* h_s/\nu$.

(ii) The law of the wall is modified by the shear stress gradient parameter μ but not by $Re^{*\prime}$. The additive constant B of the log-law, however, increases or decreases with the decrease in the absolute value of μ for the negative or positive value, respectively, depending on its sign. Such μ dependence of the wall law can be explained by the change in the production rate of turbulent kinetic energy with μ in the buffer layer.

(iii) A half-power representation of the velocity profile can be given on the basis of the characteristic velocity scale u_s^* and the length scale h_s in the region where the shear stress gradient has primary importance. The constant K_1 in equation (15) is influenced not only by $\beta' = \alpha h_s/u_s^{*2}$ but also by $Re^{*\prime}$.

(iv) It is appropriate that the defect law in the turbulent core region is given by equation (16). For P-type flow, the characteristic velocity scale u_e^* and the length scale h_s are recommended. On the other hand, the characteristic velocity scale u_c^* and the length scale h are recommended for C-type flow.

(v) Similarity laws for the turbulence intensity variation in the wall region normalized by wall variables can be expressed as functions of $Re^{*\prime}$ and shear stress gradient parameter μ, equations (19), (21) and (22). Those in the turbulent core region can be expressed by the characteristic velocity scale u_e^* and the length scale h_s for P-type flow, but by the characteristic velocity scale u_c^* and the length scale h for C-type flow, equations (23) and (24), respectively. Similar laws also hold for the skewness factor. The experimental results confirm these similarity laws. In the wall region, μ is a governing parameter whereas $Re^{*\prime}$ has little effect on the similarity law.

(vi) Because the relation $\mu = -Re^{*\prime} = -Re^*$ holds for plane Poiseuille flow and $Re^{*\prime}$ or Re^* has little effect on the similarity laws for C-P flows, the low Reynolds number effect on mean velocity and turbulence quantities can be attributed to μ effect for plane Poiseuille flow.

(vii) The turbulence activity away from the wall is extremely high for $\mu > 0$, but low for $\mu < 0$. Thus, a strong sweep plays a dominant role in the Reynolds shear stress when $0 < \mu < 50$, whereas strong ejection from the near-wall region prevails in the case of negative μ with a small absolute value.

This work was supported through a Grant-in-Aid (No. 03452123) in 1991–1995 by the Japan Ministry of Education, Science, Sports and Culture.

REFERENCES

Andersson, H. I., Bech, K. H. & Kristoffersen, R. 1993 Reynolds-stress budgets in plane Couette flow: direct simulation and second moment modelling. *Proc. 2nd Intl Symp. on Engineering Turbulence Modelling and Experiments* (Ed. W. Rodi & F. Martelli) pp. 293–302. Elsevier.

Antonia, R. A., Teitel, M., Kim, J. & Brown, L. W. B. 1992 Low Reynolds number effects in a fully developed turbulent channel flow. *J. Fluid Mech.* **236**, 579–605.

Bahtia, J. C., Durst, F. & Jovanovic, J. 1982 Correlation of hot-wire anemometer measurements near walls. *J. Fluid Mech.* **122**, 411–431.

Bech, K. H., Tillmark, N., Alfredsson, P. H. & Andersson, H. I. 1995 An investigation of turbulent Couette flow at low Reynolds number. *J. Fluid Mech.* **177**, 133–166.

Blackwelder, R. F. & Kovasznay, L. S. G. 1972 Large-scale motion of a turbulent boundary layer. *J. Fluid Mech.* **53**, 61–83.

Dean, R. B. 1978 Reynolds number dependence of skin friction and other bulk flow variables in two dimensional rectangular duct flow. *Trans. ASME: J. Fluids Engng* **100**, 215–233.

El Telbany, M. M. M. & Reynolds, A. J. 1980 Velocity distributions in plane turbulent channel flows. *J. Fluid Mech.* **100**, 1–29.

El Telbany, M. M. M. & Reynolds, A. J. 1981 Turbulence in plane channel flows. *J. Fluid Mech.* **111**, 283–318.

Horiuti, K. 1993 Establishment of the direct numerical simulation data bases of turbulent transport phenomena. *Co-operative Research No. 02302043 supported by the Ministry of Education, Science and Culture, Japan*, 1990–1992.

Huffman, G. K. & Bradshaw, P. 1972 A note on von-Karman's constant in low Reynolds number turbulent flows. *J. Fluid Mech.* **53**, 45–60.

Hussain, A. K. M. F. & Reynolds, W. C. 1975 Measurements in fully developed turbulent channel flow. *Trans. ASME: J. Fluids Engng* **97**, 568–580.

Johansson, A. V. & Alfredsson, P. H. 1982 On the structure of turbulent channel flow. *J. Fluid Mech.* **122**, 295–314.

Kader, B. A. & Yaglom, A. M. 1978 Similarity treatment of moving-equilibrium turbulent boundary layers in adverse pressure gradients. *J. Fluid Mech.* **89**, 305–343.

Kays, W. M. 1971 Heat transfer to the transpired turbulent boundary layer. *ASME Paper* 71-HT-44.

Kim, J., Moin, P. & Moser, R. 1987 Turbulence statistics in fully developed channel flow at low Reynolds number. *J. Fluid Mech.* **177**, 133–166.

KITOH, O. & NAKABAYASHI, K. 1993 Reynolds number effect on turbulent characteristics of fully developed turbulent flow. *Trans. Japan Soc. Mech. Engng* **59**-564 B, 2443–2449.

KREPLIN, H. P. & ECKELMANN, H. 1979 Behavior of the three fluctuating velocity components in the wall region of a turbulent channel flow. *Phys. Fluids* **22**, 1233–1239.

KURODA, A. 1990 Direct numerical simulation of Couette–Poiseuille flows. PhD thesis, University of Tokyo.

KURODA, A., KASAGI, N. & HIRATA, M. 1994 Direct numerical simulation of turbulent Couette-Poiseuille flows: Effect of mean shear rate on the near-wall turbulent structures. *Turbulent Shear Flows 9* (ed. F. Durst *et al.*), pp. 241–257. Springer.

LEE, M. J. & KIM, J. 1991 The structure of turbulence in a simulated plane Couette flow. *Proc. 8th Symp. Turbulent Shear Flows*, pp. 5-3-1–5-3-6.

NAGANO, Y., TAGAWA, M. & TSUJI, T. 1991 Effects of adverse pressure gradients on mean flows and turbulence statistics in a boundary layer. *Turbulent Shear Flows 8* (ed. F. Durst *et al.*), pp. 7–21. Springer.

NAKABAYASHI, K., KITOH, O., ADACHI, M. & IKEYA, T. 1994 Turbulent structure in plane Couette flow. *Trans. Japan Soc. Mech. Engng* **60**-578 B, 3249–3255.

NAKABAYASHI, K., KITOH, O., IWATA, Y., KATO, E. & UEHARA, T. 1988 Basic study on turbulent lubrication (1st report, Turbulent plane Couette flow). *Trans. Japan Soc. Mech. Engng* **54**-499 B, 547–552.

NAKABAYASHI, K., KITOH, O. & NISHIMURA, F. 1997 Experimental study of a turbulent Couette flow at low Reynolds number. *Proc. 11th Symp. Turbulent Shear Flows, Grenoble*, pp. 11-10–11-15.

NISHINO, K. & KASAGI, N. 1990 Turbulence statistics measurement in a two-dimensional turbulent channel flow with the aid of the three-dimensional particle tracking velocimeter. *Trans. Japan Soc. Mech. Engng* **56**-525 B, 1338–1347.

PATEL, V. C. & HEAD, M. R. 1969 Some observations on skin friction and velocity profiles in fully developed pipe and channel flows. *J. Fluid Mech.* **38**, 181–201.

PERRY, A. E. & ABELL, C. J. 1975 Scaling laws for pipe flow turbulence. *J. Fluid Mech.* **67**, 257–271.

REICHARDT, H. 1959 Gesetzmässigkeiten der geradlinigen turulenten Couetteströmung. *Mitt. Max Planck Institut fur Strömungsforschung*. **22**, 1–45.

ROBERTSON, J. M. 1959 On turbulent plane-Couette flow. *Proc. 6th Midwestern Conf. Fluid Mech. Univ. Texas. Austin*, pp. 169–182.

SAMUEL, A. E. & JOUBERT, P. N. 1947 A boundary layer developing in an increasingly adverse pressure gradient. *J. Fluid Mech.* **66**, 481–505.

TAVOULARIS, S. & KARNIK, K. 1989 Further experiments on the evolution of turbulent stresses and scales in uniformly sheared turbulence. *J. Fluid Mech.* **204**, 457–478.

THURLOW, E. M. & KLEWICKI, J. C. 2000 Experimental study of turbulent Poiseuille-Couette flow. *Phys. Fluids* **12**, 865–875.

WEI, T. & WILLMARTH, W. W. 1989 Reynolds number effects on the structure of turbulent channel flow. *J. Fluid Mech.* **204**, 57–95.